Advanced Powder Technology 26 (2015) 935–946

Contents lists available at ScienceDirect

Advanced Powder Technology

journal homepage: www.elsevier.com/locate/apt

Original Research Paper

Theoretical analysis of natural convection boundary layer heat and mass transfer of nanofluids: Effects of size, shape and type of nanoparticles, type of base fluid and working temperature

Abolfazl Zaraki [a], Mohammad Ghalambaz [b,*], Ali J. Chamkha [c], Mehdi Ghalambaz [b], Danilo De Rossi [a]

[a] Research Center "E. Piaggio", University of Pisa, Italy
[b] Department of Mechanical Engineering, Dezful Branch, Islamic Azad University, Dezful, Iran
[c] Mechanical Engineering Department, Prince Mohammad Bin Fahd University (PMU), P.O. Box 1664, Al-Khobar 31952, Saudi Arabia

ARTICLE INFO

Article history:
Received 17 September 2014
Received in revised form 18 February 2015
Accepted 26 March 2015
Available online 7 April 2015

Keywords:
Size of nanoparticles
Shape of nanoparticles
Working temperature
Drift-flux model

ABSTRACT

The problem of natural convection boundary layer heat transfer of nanofluids is theoretically analyzed. Different aspects of nanoparticles, such as size, shape and constructive material, as well as the type of the base fluid and the working temperature, are examined. The drift-flux model of nanofluids, including the effects of Brownian motion, thermophoresis, and the local volume fraction of nanoparticles, is adopted to model the boundary layer heat and mass transfer of nanofluids. Following the state-of-the-art, the thermo-physical properties are extracted from five different synthesized types of nanofluids. A new non-dimensional parameter, the enhancement ratio, indicating the ratio of the convective heat transfer coefficient of the nanofluid to the base fluid, is introduced. The effect of the nanoparticles on the enhancement of natural convective heat transfer of nanofluids is discussed. The main findings of this study are as follows: (i) the type of the nanoparticles and the base fluid are the most important parameters affecting the heat transfer of nanofluids; (ii) in some cases, the presence of nanoparticles in the base fluid deteriorates the heat transfer rate; and (iii) the rise of the working temperature reduces the efficiency of the nanofluid, which is a crucial issue in applications of nanofluids as coolants.

1. Introduction

Nanofluids are a new type of engineered heat transferred fluids, containing nano-sized solid nanoparticles that are being used to enhance the heat transfer [1]. The thermal conductivity and the dynamic viscosity of nanofluids are the most important thermo-physical properties, which affect the convective heat transfer performance of nanofluids [2]. The experiments show that the thermal conductivity and the dynamic viscosity of nanofluids are functions of the size, the shape, and the constructive materials of nanoparticles, as well as the type of the base fluid and the working temperature of the nanofluid [3–7]. There are also other affective parameters such as the method of synthesis of the nanofluids, the sonication time, which affect the thermo-physical properties and the heat transfer performance of nanofluids [4,6,8]. In addition, there are mass transfer mechanisms, such as Brownian motion and thermophoresis effects, which influence the convective heat transfer performance of nanofluids [9,10].

There are many experimental reports, which have measured the thermal conductivity or the dynamic viscosity of synthesized nanofluids. In order to theoretically analysis the convective heat transfer of nanofluids, the thermal conductivity and the dynamic viscosity of a nanofluid as functions of the volume fraction of nanoparticles are required simultaneously. However, only few studies have reported the data of the thermal conductivity and the dynamic viscosity of a nanofluid, simultaneously [11–15]. Some of these studies are as follows:

Chandrasekar et al. [11] measured the thermal conductivity and the dynamic viscosity of water–Al_2O_3 nanofluids. They dispersed powders of 43 nm spherical alumina nanoparticles in the water, and then sonicated the nanofluid for 6 h. The thermal conductivity was measured using the hot wire method, and the dynamic viscosity was measured using the Brookfield cone and plate viscometer. The measurements were performed at room temperature. The results indicated the Newtonian behaviors of the samples. It was

* Corresponding author. Tel.: +98 916 644 2671.
E-mail addresses: a.zaraki@centropiaggio.unipi.it (A. Zaraki), m.ghalambaz@iaud.ac.ir (M. Ghalambaz), achamkha@pmu.edu.sa (A.J. Chamkha), ghalambaz.mehdi@gmail.com (M. Ghalambaz), d.derossi@centropiaggio.unipi.it (D. De Rossi).

http://dx.doi.org/10.1016/j.apt.2015.03.012
0921-8831/

Nomenclature

c	specific heat in constant pressure (J/kg K)
D_B	Brownian diffusion coefficient (m^2/s)
D_T	thermophoretic diffusion coefficient (m^2/s)
f	rescaled nanoparticle volume fraction, nanoparticle concentration
g	gravitational acceleration (m/s^2)
h	thermal convective coefficient (W/m^2 K)
j_p	drift flux of nanoparticles
k	thermal conductivity coefficient (W/m K)
Le	Lewis number
Nb	Brownian motion parameter
Nc	conductivity parameter
Nr	buoyancy ratio
Nt	thermophoresis parameter
Nu	Nusselt number
Nv	viscosity parameter
P	pressure (Pa)
Pr	Prandtl number
Ra	Rayleigh number
S	dimensionless stream function
T	temperature (°C)
u	non dimensional velocity component in x-direction (m/s)
v	non dimensional velocity component in y-direction (m/s)
x	Cartesian coordinate in horizontal direction (m)
y	Cartesian coordinate in vertical direction (m)

Greek symbols

μ	thermal viscosity (kg s/m)
α	thermal diffusivity (m^2/s)
β	thermal expansion coefficient (1/K)
η	dimensionless distance
θ	non dimensional temperature
ρ	density (kg/m^3)
ϕ	volume fraction of nanoparticles
ψ	stream function

Subscript

∞	outside the boundary layer
bf	base fluid
nf	nanofluid
p	nanoparticles
w	wall

Superscript

$'$	differentiation respect to η

also found that the increase of the volume fraction of nanoparticles increased the thermal conductivity and the dynamic viscosity of the nanofluid.

Duangthongsuk and Wongwises [12] measured the thermal conductivity and the dynamic viscosity of water-based nanofluids, synthesized by 21 nm spherical nanoparticles of TiO_2. The thermal conductivity and the dynamic viscosity of the samples were measured by using the hot wire method and the rotational rheometer at three selected working temperatures of 15 °C, 25 °C and 35 °C. The results of this study also indicate the Newtonian behavior of the samples. The results revealed that the thermal conductivity of the nanofluid was a decreasing function of the working temperature while the dynamic viscosity of the nanofluid was an increasing function of the working temperature.

Jeong et al. [13] studied the effect of the shapes of nanoparticles on the thermal conductivity and the dynamic viscosity of nanofluids. The authors synthesized two types of water-based nanofluids using nanopowers of rectangular (150 nm) and spherical (40 nm) zinc-oxide nanoparticles. The nanoparticles were well dispersed in the base fluid by the aid of the ultrasonic method. The dynamic viscosity and the thermal conductivity of the samples were measured at room temperature using the hot wire method and Ubbelohde viscometer, respectively. The results indicated that the thermal conductivity and the dynamic viscosity of the nanofluid containing rectangular nanoparticles were higher than those containing the spherical nanoparticles. However, the size of the spherical nanoparticles was much smaller than that of the rectangular ones.

Esfe et al. [14] examined the thermal conductivity and the dynamic viscosity of manganese-oxide water-based nanofluids at the room temperature. The nanofluid was synthesized using a powder of 40 nm spherical nanoparticles. The nanoparticles were dispirited in the water using the ultrasonic waves. The thermal conductivity and the dynamic viscosity of the samples were measured by using the hot wire method and Brookfield viscometer, respectively. The results showed that the increase of the volume fraction of the nanoparticles increased the thermal conductivity and the dynamic viscosity of the nanofluid.

Agarwal et al. [15] studied the influence of the size of nanoparticles on the thermal conductivity and the dynamic viscosity of nanofluids. They synthesized two types of kerosene–Al_2O_3 nanofluids using powders of spherical alumina nanoparticles with two sizes of 21 nm and 44 nm. The nanoparticles were well dispersed in the kerosene utilizing the ultrasonic waves. The thermal conductivity and the dynamic viscosity of the nanofluids were measured at room temperature using the hot wire and the Brookfield viscometer, respectively. The results indicated that the thermal conductivity and the dynamic viscosity of the samples of nanofluids containing smaller size of nanoparticles (21 nm particles) were higher than those containing larger size of nanoparticles (44 nm particles).

As a benchmark study, Buongiorno et al. [16] and Venerus et al. [17] have analyzed the effect of volume fraction of nanoparticles on the thermal conductivity and dynamic viscosity of nanofluids for different samples of nanofluids in 30 different laboratories around the world using different measurement methods. The results indicated that the thermal conductivity and dynamic viscosity of nanofluids are linear functions of the volume fraction of nanoparticles for low volume fractions of nanoparticles. Therefore, the linear function of concentration of particles for conductivity and viscosity is valid only in low concentrations of nanoparticles, and for high concentration of nanoparticles non-linear relations are required.

In the present study, the results of the measured thermal conductivity and dynamic viscosities of nanofluids reported by the previous researchers [11–15] are utilized to analysis the different aspects of nanoparticles and base fluids on the convective heat transfer of nanofluids.

Rana and Bhargava [18], using a homogenous model, examined natural convection heat transfer of nanofluids over a vertical flat plate. They investigated the effect of the presence of different types of nanoparticles (silver, copper, copper oxide, alumina, and

titanium oxide) on the boundary layer heat transfer of water-based nanofluids. The Maxwell model and the Brinkman model were utilized to model the thermal conductivity and the dynamic viscosity of the nanofluids, respectively. The results indicated that the presence of nanoparticles increased the heat transfer rate. The highest enhancement was achieved for the silver nanoparticles. However, the effects of the sizes of the nanoparticles, the shape of nanoparticles and the working temperature cannot be seen in the Maxwell and Brinkman models. Therefore, these effects have not been examined in the study of Rana and Bhargava [18]. It is worth noticing that the mass transfer mechanism, including the Brownian motion and the thermophoresis effects, are neglected in the homogeneous model of Rana and Bhargava [18].

Kuznetsov and Nield [9] studied natural convection heat transfer of nanofluids over an isothermal flat plate. They assumed a constant volume fraction of nanoparticles at the surface, which is possible by an active control of volume fractions of nanoparticles at the surface of the plate. The presence of a concentration boundary layer of nanoparticles was taken into account, due to the Brownian motion and the thermophoresis effects. Aziz and Khan [19] as well as Uddin et al. [19] extended the study of Kuznetsov and Nield [9] to the case of natural convection boundary layer heat transfer of nanofluids over a flat plate, which was subject to a convective heat transfer boundary condition. Later on, Kuznetsov and Nield [21] proposed a new enhanced boundary condition for the volume fraction of nanoparticles at the surface of the plate. Using the enhanced boundary condition, the mass flux of nanoparticles at the surface of the plate is zero, and the volume fraction of nanoparticles can be adjusted passively at the surface of the plate by the boundary layer. This new boundary condition is in better agreement with the practical applications of nanofluids. In the study of Kuznetsov and Nield [21] as well as the studies of Aziz and Khan [19] and Uddin et al. [20], the effect of the local variation of the thermo-physical properties due to the migration of nanoparticles were neglected. In these studies, the results were reported in a general non-dimensional form, and hence, the different aspects of nanoparticles, or the base fluid were not discussed.

To the best of the authors' knowledge, the effects of size, shape, and type of nanoparticles, the type of the base fluid and the working temperature have not yet been investigated for the heat transfer boundary layer of nanofluid while these parameters are very important in the synthesis of nanofluids [3,5–8,22–24]. In addition, there is no theoretical study to report the effect of mass transfer of nanoparticles on the heat transfer of nanofluids in the boundary layer for practical case studies.

In this study, the effects of size, shape, and type of nanoparticles as well as the types of the base fluid and the working temperature on the heat transfer performance of nanofluids in natural convection boundary layer heat transfer applications are examined. The new enhanced boundary condition, the zero mass flux of nanoparticles at the surface, is utilized. In addition, the effect of the mass transfer mechanism of nanoparticles because of the Brownian motion and thermophoresis on the local volume fraction of nanoparticles and buoyancy forces is theoretically analyzed and the results are reported for practical case studies. The effect of thermal conductivity and dynamic viscosity are being linearized and analyzed in the form of two new non-dimensional parameters of dynamic viscosity and thermal conductivity parameters.

2. Mathematical model

Consider a two-dimensional steady-state boundary layer flow and heat transfer of a nanofluid over an isothermal vertical flat plate. The hot plate with uniform temperature of T_w is placed in a quiescent nanofluid at the temperature of T_∞ and a uniform

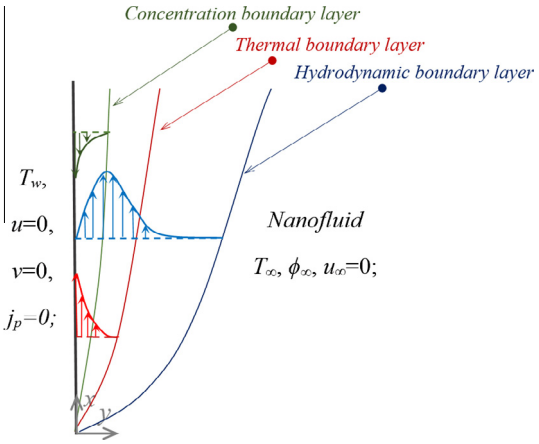

Fig. 1. The schematic view of the flat plate in a nanofluid.

volume fraction of nanoparticles ϕ_∞. The geometry of the flat plate is chosen in the present study as a benchmark geometry, which indicates the general behaviors of external flows. In addition, there are numerous industrial and physical applications for natural convection heat transfer over a flat plate such as cooling of hot spot sheets immersed in nanofluid coolants. The nanofluid in the vicinity of the hot plate has a tendency to move upward because of the buoyancy force induced in the fluid. The schematic view of the physical model is depicted in Fig. 1. In addition, the presence of thermophoresis tends to move nanoparticles from the hot regions to the cold regions [9]. Therefore, the migration of heavy nanoparticles from the plate into the boundary layer induces a secondary buoyancy force in the vicinity of the plate. The migration of nanoparticles would also change the local thermo-physical properties of the nanofluid in the boundary layer.

The experiments show that the thermal conductivity and the dynamic viscosity of nanofluids are very sensitive to the variation of the volume fraction of nanoparticles [2,4–6]. Hence, the influence of the variation of the local volume fraction of nanoparticles on the thermal conductivity and the dynamic viscosity of the nanofluid are important and cannot be neglected; however, these effects have been neglected in previous studies. Here, in order to increase the physical significance of the present study, the thermal conductivity and the dynamic viscosity of nanofluids are considered as functions of the local volume fraction of nanoparticles. It is assumed that the size of nanoparticles is uniform, and the effect of the agglomeration of nanoparticles on the thermo-physical properties and the Brownian motion is neglected because of the lack of accurate physical models and experimental results.

In the present study, the following assumptions are also considered: (1) there is no chemical reaction between the nanoparticles and the base fluid. (2) The external force can be assumed by the Oberbeck-Boussinesq approximation. (3) The mixture of the base-fluid and nanoparticles is a dilute mixture. (4) The radiation heat transfer are neglected. (5) The nanoparticles and the base fluid are in local thermal equilibrium. (6) The viscous dissipation is neglected. The first assumption is applicable because the materials of nanoparticles are chosen to be in chemical inertness with the base fluid. The assumption of (2) and (6) are applicable as the nanofluids can be utilized with a limited range of the temperature differences (to avoid boiling and solidification problems), and hence, the temperature difference between the wall and the surrounding is limited. The assumption (3) is justified, as the nanofluid are synthesized with very low volume fraction of nanoparticles. The assumption (5) is realistic as the nanoparticles are very fine and conductive, and hence, they are in the same

temperature as the base fluid. Finally, the assumption (6) is accurate as the velocity magnitudes in natural convection flows are very low.

Applying the usual boundary layer approximation and considering the governing equations of the conservations of the nanofluids mass, momentum and energy and the conservation of the mass of nanoparticles are written as [21,25]:

$$\frac{\partial u_{nf}}{\partial x}+\frac{\partial v_{nf}}{\partial y}=0, \tag{1}$$

$$\rho_{nf}\left(u_{nf}\frac{\partial u_{nf}}{\partial x}+v_{nf}\frac{\partial u_{nf}}{\partial y}\right)=-\frac{\partial P_{nf}}{\partial x}+\frac{\partial\left(\mu_{nf}(\phi)\frac{\partial u_{nf}}{\partial y}\right)}{\partial y}+\left[(1-\phi_\infty)\rho_{bf,\infty}\beta_{bf}(T_{nf}-T_\infty)-\left(\rho_p-\rho_{bf,\infty}\right)(\phi-\phi_\infty)\right]g \tag{2a}$$

$$\frac{\partial P_{nf}}{\partial y}=0 \tag{2b}$$

$$(\rho c)_{nf}\left(u_{nf}\frac{\partial T_{nf}}{\partial x}+v_{nf}\frac{\partial T_{nf}}{\partial y}\right)=\frac{\partial}{\partial y}\left(k_{nf}(\phi)\frac{\partial T_{nf}}{\partial y}\right)+(\rho c)_p\left[D_B\frac{\partial\phi}{\partial y}\frac{\partial T_{nf}}{\partial y}+\frac{D_T}{T_\infty}\left(\frac{\partial T_{nf}}{\partial y}\right)^2\right] \tag{3}$$

$$u_{nf}\frac{\partial\phi}{\partial x}+v_{nf}\frac{\partial\phi}{\partial y}=D_B\frac{\partial^2\phi}{\partial y^2}+\left(\frac{D_T}{T_\infty}\right)\frac{\partial^2 T_{nf}}{\partial y^2}, \tag{4}$$

where u, v, ϕ, P and T are the x-velocity, y-velocity, volume fraction of nanoparticles, pressure and temperature of the nanofluid, respectively. The quantities of μ, β, ρ, k and c denote the dynamic viscosity, the thermal volume expansion, the density, the thermal conductivity and the specific heat capacity. D_B and D_T are the Brownian motion coefficient and the thermophoresis coefficient, respectively. The subscripts nf, bf and p denote the nanofluid, the base fluid and the nanoparticles, respectively. The subscripts of w and ∞ represent the surface of the plate and the ambient space, respectively. The drift flux of nanoparticles, j_p, is introduced as [25]:

$$j_p=-\rho_p D_B\nabla\phi-\rho_p D_T\frac{\nabla T}{T} \tag{5}$$

As the surface of the plate in impermeable, the nanoparticles cannot cross the surface of the plate, and hence, the drift flux of nanoparticles at the surface of the plate is zero, which follows that $j_p=0$. Considering the no-slip boundary condition for the velocity and the isothermal boundary condition for the energy equation, the boundary conditions at the surface of the plate are:

$$y=0:\quad u_{nf}=v_{nf}=0,\quad T=T_w,\quad j_p=0. \tag{6a}$$

Based on the problem description, far from the surface, the nanofluid is quiescent ($u_{nf}=0$) and at the uniform constant temperature of T_∞. The nanofluid far from the plate is also at uniform volume fraction of ϕ_∞. Hence, the asymptotic boundary conditions far from the plate can be written as:

$$y\to\infty:\quad u_{nf}\to 0,\quad T\to T_\infty,\quad \phi\to\phi_\infty. \tag{6b}$$

The continuity equation is satisfied by introducing the stream function as $u=\partial\psi/\partial y$ and $v=-\partial\psi/\partial x$. The pressure, between Eqs. (2a) and (2b), is eliminated by taking the cross differentiation. In order to attain a similarity solution and transforming the equations into a non-dimensional form, the similarity variables are introduced as:

$$\eta=\frac{y}{x}Ra_x^{\frac{1}{4}} \tag{7}$$

where Ra_x is the local Rayleigh number as:

$$Ra_x=\frac{\rho_{bf}g\beta_{bf}(T-T_\infty)x^3}{\mu_{bf}\alpha_{bf}} \tag{8}$$

In the above equation, α is the thermal diffusion. It is worth noticing that the thermo-physical properties of the base fluid are utilized in the definition of the Rayleigh number. Hence, the similarity variable, η, is a function of the thermo-physical properties of the base fluid, and consequently, the governing equations would be reduced to non-dimensional form with respect to the base fluid. Using this non-dimensional form, comparison between the results of the nanofluid and the base fluid is contently possible. The non-dimensional variables of the stream function (S), temperature (θ) and the concentration of nanoparticles (f) are introduced as:

$$S=\frac{\psi}{\alpha Ra_x^{\frac{1}{4}}},\quad f=\frac{\phi-\phi_\infty}{\phi_\infty},\quad \theta=\frac{T_{nf}-T_\infty}{T_w-T_\infty} \tag{9}$$

As mentioned in the Introduction section, based on the results of the benchmark studies of Buongiorno et al. [16] and Venerus et al. [17], the thermal conductivity and the dynamic viscosity of nanofluids are linear functions of the volume fraction of nanoparticles as:

$$\frac{k_{nf}}{k_{bf}}=1+Nc\times\phi \tag{10a}$$

$$\frac{\mu_{nf}}{\mu_{bf}}=1+Nv\times\phi \tag{10b}$$

In the above equations, Nc and Nv are the conductivity parameter and the viscosity parameter, respectively. These non-dimensional parameters, Nc and Nv, are generally functions of the size, shape and constructing materials of the nanoparticles, the type of the base fluid, the working temperature and other affective parameters [2,11–13]. The parameters Nc and Nv can be easily extracted using linear curve fitting on the available experimental data. Considering a specified sample of a nanofluid, these parameters, i.e. Nc and Nv, are constant. The practical values of these parameters will be discussed later. The other thermo-physical properties can be measured directly or evaluated using the averaging law. Now, invoking the similarity variables and utilizing the relations of the thermal conductivity and the dynamic viscosity (i.e. Eqs. (10a) and (10b)), the partial differential equations of the conservations of the momentum of nanofluid, and the energy of nanofluid and mass of nanoparticles (i.e. Eqs. (2)-(4)) are reduced to the following set of nonlinear ordinary differential equations:

$$\frac{1}{4Pr_{bf}}(2S'S'-3SS'')=\frac{\rho_{bf}}{\rho_{nf}}(Nv\phi_\infty f')S''+\frac{\rho_{bf}}{\rho_{nf}}(1+Nv\phi_\infty(1+f))S'''+\left[(1-\phi_\infty)\frac{\rho_{bf}}{\rho_{nf}}\theta-Nrf\right] \tag{11}$$

$$\frac{(\rho c)_{bf}}{(\rho c)_{nf}}(Nc\phi_\infty f'\theta'+(1+Nc(1+f)\phi_\infty)\theta'')+\frac{3}{4}S\theta'+Nb\times f'\theta'+Nt\theta'^2=0 \tag{12}$$

$$f''+\frac{3}{4}LeSf'+\frac{Nt}{Nb}\theta''=0, \tag{13}$$

where

$$Nr=\frac{\phi_\infty(\rho_p-\rho_{bf})}{\beta_{bf}\rho_{nf}(T_w-T_\infty)},\quad Nb=\frac{(\rho c)_p D_B\phi_\infty}{(\rho c_p)_{bf}\alpha_{bf}},\quad Nt=\frac{(\rho c_p)_p D_T(T_w-T_\infty)}{(\rho c_p)_{bf}\alpha_{bf}T_\infty},\quad Le=\frac{\alpha_{bf}}{D_B},\quad Pr_{bf}=\frac{\mu_{bf}}{\rho_{bf}\alpha_{bf}} \tag{14}$$

In the above equations, a prime denotes ordinary differentiation with respect to the similarity variable (η). *Nr*, *Nt* and *Nb* represent the non-dimensional buoyancy ratio parameter, thermophoresis parameter and the Brownian motion parameter, respectively. *Le* and *Pr* denote the Lewis number and the Prandtl number, respectively. ρ_{bf}/ρ_{nf} and $(\rho c)_{bf}/(\rho c)_{nf}$ are the density ratio and the heat capacity ratio, respectively. Using the similarity variables, the transformed boundary conditions at the surface become:

$$at\quad \eta=0:\quad S(0)=0,\quad S'(0)=0,\quad \theta(0)=1,\quad Nbf'(0)+Nt\theta'(0)=0 \tag{15}$$

The thermophoresis force is very strong in some practical cases. In these cases, adjusting the volume fraction of the nanoparticles at the surface of the plate results in a negative value for the volume fraction of nanoparticles. The negative volume fraction of nanoparticles is physically not allowed. Hence, in these cases, the zero mass flux of nanoparticles at the surface (i.e. $Nbf'(0)+Nt\theta'(0)$) is exchanged by the zero volume fraction of nanoparticles at the surface (i.e. $f(0)=-1$). The asymptotic boundary conditions of Eq. (6b) are transformed into:

$$as\quad \eta\to\infty:\quad S'(\eta)\to 0,\quad \theta(\eta)\to 0,\quad f(\eta)\to 0 \tag{16}$$

At the surface of the plate, the heat transfer by conduction, $(-k_{nf,w}\times\partial T/\partial y)$, is equal to the heat transfer by convection ($h(T_w-T_\infty)$). Hence, using the similarity variables, the local Nusselt number ($Nu_x=hx/k_{nf,\infty}$) is evaluated as:

$$Nu_x=-\frac{k_{nf,w}}{k_{bf}}\theta'_{nf}(0)Ra_x^{\frac{1}{4}} \tag{17}$$

where $k_{nf,w}$, $k_{nf,\infty}$ k_{bf} are the thermal conductivity of the nanofluid at the plate, the thermal conductivity of the nanofluid at the ambient space, and the thermal conductivity of the base fluid. Invoking Eq. (10a), the reduced Nusselt number (*Nur*) is evaluated as:

$$Nur=Nu_xRa_x^{-\frac{1}{4}}=-(1+\phi_\infty Nc(1+f(0)))\theta'_{nf}(0) \tag{18}$$

Finally, an important non-dimensional heat transfer parameter, which indicates the heat transfer enhancement of using nanofluids in comparison with the base fluid, is introduced as:

$$\frac{h_{nf}}{h_{bf}}=(1+\phi_\infty Nc(1+f(0)))\frac{\theta'_{nf}(0)}{\theta'_{bf}(0)} \tag{19}$$

where h_{nf}/h_{bf} is the enhancement ratio, which indicates the robustness of dispersing nanoparticles in natural convection heat transfer applications. An enhancement ratio higher than unity indicates an increase in the convection heat transfer by using nanoparticles. On the other hand, an enhancement ratio lower than unity indicates that the presence of the nanoparticles deteriorates the natural convection heat transfer.

3. Numerical method and code validation

The obtained Ordinary Differential Equations (ODES) of Eqs. (11)–(13) are written as a system of first-order ODEs as:

$$\begin{aligned}
y'_1&=y_2\\
y'_2&=y_3\\
y'_3&=-\frac{-\frac{1}{4Pr_{bf}}(2y_2^2-3y_1y_3)+\frac{\rho_{bf}}{\rho_{nf}}(N\nu\phi_\infty y_7)S''+(1-\phi_\infty)\frac{\rho_{bf}}{\rho_{nf}}y_4-Nry_6}{\frac{\rho_{bf}}{\rho_{nf}}(1+N\nu\phi_\infty(1+y_6))}\\
y'_4&=y_5\\
y'_5&=-\frac{\frac{3}{4}y_1y_5+Nb\times y_7y_5+Nty_5^2-\frac{(\rho c)_{bf}}{(\rho c)_{nf}}Nc\phi_\infty y_7y_5}{\frac{(\rho c)_{bf}}{(\rho c)_{nf}}(1+Nc(1+y_6)\phi_\infty)}\\
y'_6&=y_7\\
y'_7&=-\frac{3}{4}LeSf'+\frac{Nt}{Nb}\frac{\frac{3}{4}y_1y_5+Nb\times y_7y_5+Nty_5^2-\frac{(\rho c)_{bf}}{(\rho c)_{nf}}Nc\phi_\infty y_7y_5}{\frac{(\rho c)_{bf}}{(\rho c)_{nf}}(1+Nc(1+y_6)\phi_\infty)}
\end{aligned} \tag{20}$$

The boundary conditions, at the surface of the plate and far from the plate, are written as:

$$\eta=0:\quad y_1(0)=0,\quad y_2(0)=0,\quad y_4(0)=1,\quad Nby_7(0)+Nty_5(0)=0 \tag{21}$$

$$\eta\to\infty:\quad y_2(\eta)\to 0,\quad y_4(\eta)\to 0,\quad y_6(\eta)\to 0 \tag{22}$$

The system of Eqs. (20) associated with the boundary conditions (21) and (22) is numerically solved by means of the finite-difference method. The 3-stage Lobatto IIIa is applied; the collocation method with an automatic mesh adaptation scheme is also utilized to uniform the error in the domain of the solution. The details of the applied numerical method can be found in the work of Ascher et al. [26] and Russel and Shampine [27]. The equations were integrated with the relative error of 10^{-8}. The physical asymptotic value of $\eta_\infty=10$ is selected as the finite value at infinity. Later, the physical asymptotic value, η_∞, is raised until the results do not change. In addition, plotting the results, visually confirms that the boundary layer profiles tend to the corresponding boundary conditions at infinity asymptotically.

As mentioned, very recently, Kusnetsov and Nield [21] examined natural convection boundary layer heat transfer of nanofluids. They neglected the effect of local volume fraction of nanoparticles on the boundary layer heat transfer of nanofluid. By assuming $Nc=0$, $Nv=0$, $\rho_{bf}/\rho_{nf}=1.0$ and $(\rho c)_{bf}/(\rho c)_{nf}=1.0$, the present study

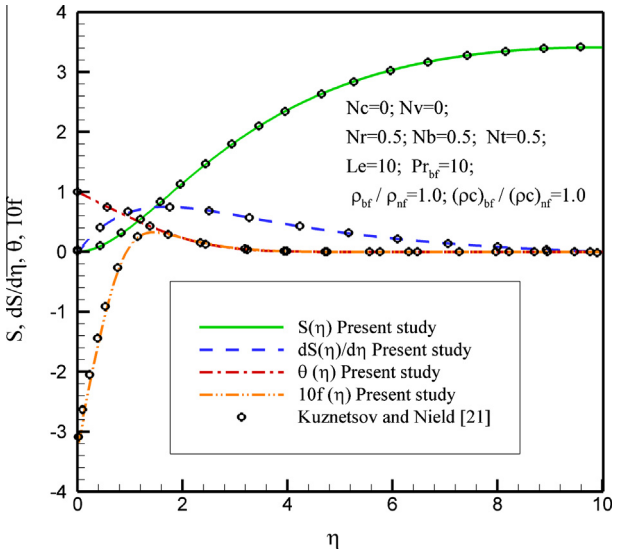

Fig. 2. A comparison between the boundary layer profiles calculated in the present study and those reported by Kusnetsov and Nield [21].

reduces to the study of Kusnetsov and Nield [21]. In this case, the results of the present study and the results reported by Kusnetsov and Nield [21] are plotted in Fig. 2. This figure indicates that there is a very good agreement between the results of the present study and that of Kusnetsov and Nield [21].

4. Results and discussion

In this section, the influence of the presence of the nanoparticles on the natural convection boundary heat and mass transfer of nanofluids are analyzed. Five experimental studies and a total number of nine different types of nanofluids, which their data of thermal conductivity and dynamic viscosity are available, are selected. Then, the practical values of the thermal conductivity and the dynamic viscosity parameters, i.e. *Nc* and *Nv*, are evaluated using linear interpolation on the available data of the nanofluids. The results are summarized in Table 1. Table 1 shows the values of *Nc* and *Nv* for nine different samples of nanofluids which are extracted from the available experimental studies. By comparison between the enhancement ratios of these different samples, the influence of the size, shape, type of nanoparticles, type of the base fluid and the working temperature on the boundary layer heat transfer of nanofluids is analyzed. The room temperature is considered as 25 °C. The corresponding thermo-physical properties of the base fluids and the nanoparticles of Table 1 are brought in Tables 2 and 3, respectively. Table 1 indicates that the thermal conductivity and dynamic viscosity of the kerosene is very sensitive to the presence of alumina nanoparticles. As seen in Table 1, the dynamic viscosity of the rectangular nanoparticles is higher than that of the spherical ones. Compared to the sphere shape, the nearly rectangular shape is hard to rotate, and hence, the flow resistance and also the viscosity for this type of nanofluid is higher. Table 4 shows that the highest values of the Brownian motion parameter (*Nb*) corresponds to kerosene–alumina nanofluid containing 21 nm spherical nanoparticles. This is because of the size of nanoparticles. As the size of nanoparticles decreases, the Brownian motion increases. Table 4 indicates that the buoyancy ratio parameter (*Nr*) for the case of water–ZnO nanofluids is more significant than the other studied nanofluids. This is because of the high density of zinc oxide nanoparticles. The migration of very heavy nanoparticles induces strong buoyancy forces because of the nanoparticles mass transfer.

For each sample of the nanofluids, using the results of Tables 1–3, the non-dimensional parameters of Eq. (20) are evaluated, and then, the governing equations are solved numerically. For example, the non-dimensional parameters for the nine different types of nanofluids samples of Table 1 with the fixed nanoparticles volume fraction of $\phi_\infty = 3\%$ are shown in Table 4. In the following sections, the boundary layer profiles are reported for a 3% volume fraction of nanoparticles, corresponding to the non-dimensional parameters of Table 4.

Table 3
Thermo-physical properties of nanoparticles [23,30].

Type	Density (kg/m^3)	Thermal conductivity (W/m^2 K)	Specific heat capacity (J/kg K)	Thermal diffusive (m^2/s)	Volume thermal expansion (1/K) × 10^{-6}
Al_2O_3	3950	40	773	1.310	17.4
TiO_2	4250	8.4	692	0.286	12.2
ZnO	5700	25	523	0.581	8.7
MgO	3580	30	879	0.953	33.6

Table 4
The non-dimensional parameters at a 3% volume fraction of nanoparticles.

Case	$Nb \times 10^{+7}$	$Nt \times 10^{+6}$	$Le \times 10^{-4}$	Nr	ρ_{bf}/ρ_{nf}	$(\rho c)_{bf}/(\rho c)_{nf}$
1	26.4445	94.8599	0.7979	74.8599	0.9111	1.0090
2	33.8936	71.6928	0.6244	39.5701	0.9108	1.0089
3	42.2718	55.9889	0.5025	27.7692	0.9105	1.0088
4	4.80980	26.6484	4.4600	55.0219	0.8760	1.0086
5	18.0367	26.6484	1.1893	55.0219	0.8760	1.0086
6	19.0394	23.6235	1.1893	32.0077	0.9279	1.0074
7	17.1850	17.3599	1.2785	36.2185	0.9184	1.0081
8	133.621	35.4886	0.4317	10.7143	0.8929	0.9731
9	63.7736	35.4886	0.9046	10.7143	0.8929	0.9731

4.1. Size of nanoparticles

The influence of the size of nanoparticles on the boundary layer heat and mass transfer can be analyzed by comparing the results of samples of S8 and S9, which correspond to alumina nanoparticles with sizes of 21 nm and 44 nm, respectively. Figs. 3 and 4 depict the non-dimensional velocity and the non-dimensional temperature profiles of these two nanofluids, respectively. Fig. 5 shows the volume fraction distribution of nanoparticles in the boundary layer. As a comparison, the non-dimensional velocity and the non-dimensional temperature profiles of the base fluid (kerosene)

Table 1
The evaluated value of *Nc* and *Nv* for different samples of nanofluids.

Case	Refs.	Temperature (°C)	Type	Base fluid	Size (nm)	Shape	*Nc*	*Nv*
1	[12]	15	TiO_2	Water	21	Spherical	4.25	4.47
2	[12]	25	TiO_2	Water	21	Spherical	3.87	7.65
3	[12]	35	TiO_2	Water	21	Spherical	3.42	9.57
4	[13]	25	ZnO	Water	150	Rectangular	3.86	13.20
5	[13]	25	ZnO	Water	40	Spherical	3.26	10.88
6	[14]	25	MgO	Water	40	Spherical	7.70	12.05
7	[11]	25	Al_2O_3	Water	43	Spherical	3.37	16.68
8	[15]	25	Al_2O_3	Kerosene	21	Spherical	20.1	20.23
9	[15]	25	Al_2O_3	Kerosene	44	Spherical	14.1	15.62

Table 2
Thermo-physical properties of water and kerosene [28,29].

Type	Temperature (°C)	Density (kg/m^3)	Specific heat capacity (J/kg K)	Volume thermal expansion (1/K) × 10^{-4}	Dynamic viscosity (Pa s)	Thermal conductivity (W/m^2 K)	Thermal diffusive (m^2/s)	Prandtl
Water	15	999.10	4185.5	1.188	11.40	0.588	1.406	8.117
Water	25	997.05	4181.4	2.253	8.93	0.606	1.454	6.161
Water	35	994.04	4178.4	3.222	7.21	0.622	1.499	4.837
Kerosene	25	790.00	2010.0	10.000	14.11	0.101	0.631	28.10

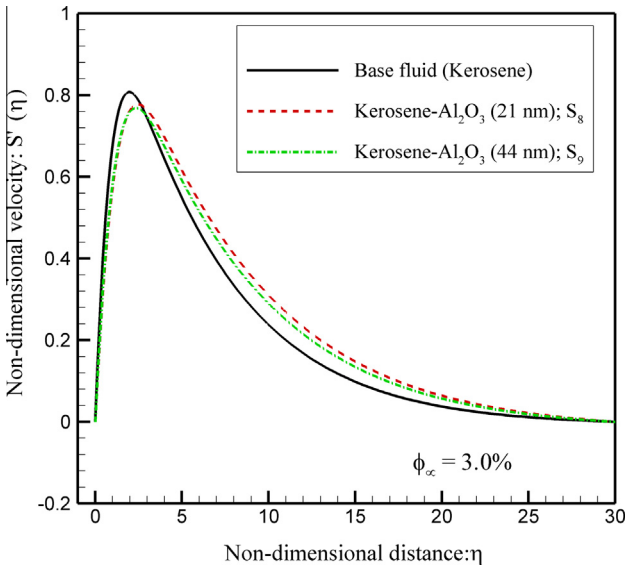

Fig. 3. A comparison between the velocity profiles of kerosene–Al_2O_3 nanofluids.

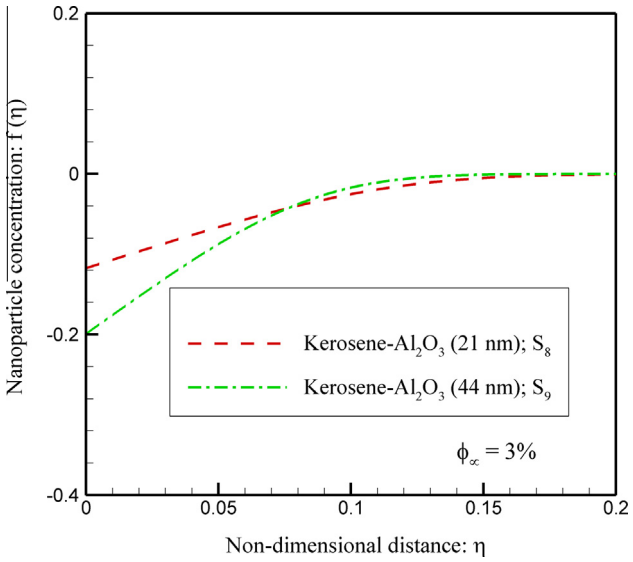

Fig. 5. A comparison between the concentration profiles of kerosene–Al_2O_3 nanofluids.

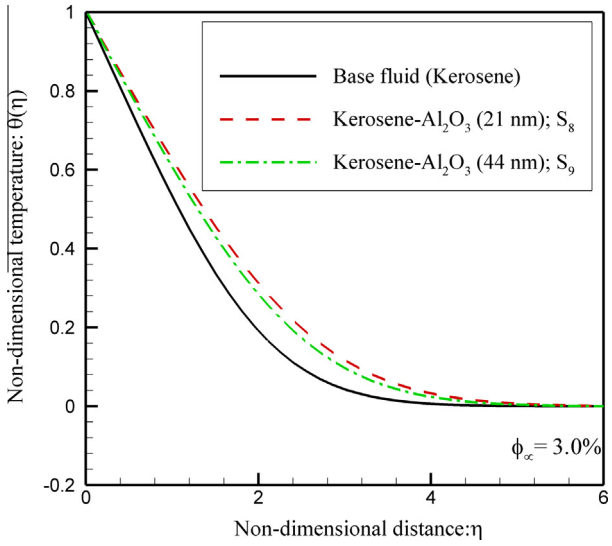

Fig. 4. A comparison between the temperature profiles of kerosene–Al_2O_3 nanofluids.

are also plotted in Figs. 3 and 4. As seen, the maximum velocities of the nanofluids are lower than that of the base fluid. The thicknesses of the hydrodynamic boundary layers of the nanofluids are higher than that of the base fluid. The decrease in the maximum velocity of the nanofluids (compared to that of the base fluid) is due to the increase in the viscosity of the nanofluids due to the presence of the nanoparticles. In the regions near the plate, the shear stress forces are dominant, and hence, the increase in the dynamic viscosity of the nanofluid decreases the maximum velocity of the nanofluid. The increase of the thickness of the hydrodynamic boundary layer of the nanofluid (compared to that of the base fluid) is due to the higher viscosity of the nanofluid in comparison with that of the base fluid. As the viscosity parameter of the nanofluid containing 21 nm nanoparticles (S8) is higher than that containing 44 nm nanoparticles (S9), the thickness of the hydrodynamic boundary layer of S8 is higher than that of S9. Fig. 4 shows that the thicknesses of the thermal boundary layer of the nanofluids are higher than that of the base fluid. The increase of the thicknesses of the thermal boundary layer of the nanofluids is due to the higher thermal conductivity of these fluids. As seen, the thickness of the thermal boundary layer of the nanofluid containing 21 nm alumina nanoparticles (S8) is higher than that containing 44 nm (S9). Table 1 also depicts that *Nc* of S8 is higher than that of S9. Fig. 5 indicates that the volume fraction of the nanofluid synthesized by 44 nm nanoparticles at the surface of the plate is lower than the nanofluid with 21 nm nanoparticles. Based on the non-dimensional parameters of Table 4, the thermophoresis parameters of these two nanofluids are the same, but the Brownian motion parameter of the nanofluid containing 21 nm nanoparticles is higher than that of the 44 nm nanoparticles. Indeed, the lower size of the nanoparticles is, the higher the Brownian motion effects. Fig. 5 also depicts that the thickness of the concentration boundary layer of S9 is higher than that of S8. This is because of the differences between the Lewis numbers of these two nanofluids. Table 4 shows that the Lewis number of the nanofluid containing 44 nm alumina nanoparticles (S9) is higher than that of the nanofluid containing 21 nm alumina nanoparticles (S8). Therefore, the thickness of the concentration boundary layer of the nanofluid of S8 is higher than that of S9.

Fig. 6 shows the enhancement ratio of alumina–kerosene nanofluids as a function of the volume fraction of nanoparticles. This figure reveals that the presence of the nanoparticles in the base fluid enhances the overall natural convection heat transfer. The smaller the nanoparticles are, the higher the enhancement ratio. It is clear that the increase of the volume fractions of nanoparticles increases the enhancement ratio.

4.2. Shape of nanoparticles

The influence of the shape of nanoparticles on the boundary layer profiles and the enhancement ratio parameter is analyzed by performing a comparison between S4 (rectangular ZnO nanoparticles in water) and S5 (spherical nanoparticles in water). Figs. 7 and 8 show the non-dimensional velocity and the non-dimensional temperature profiles of water–ZnO nanofluids, respectively. Fig. 7 shows that the maximum velocity of the nanofluid containing the spherical nanoparticles (S5) is higher than that containing the rectangular ones (S4), but the thickness of the hydrodynamic boundary layer of the nanofluid synthesized by rectangular

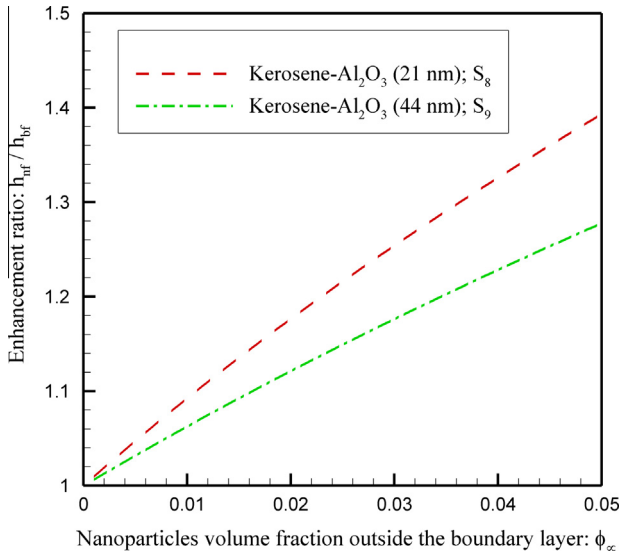

Fig. 6. Enhancement ratio of alumina–kerosene nanofluids (S8 and S9) as a function of the volume fraction of nanoparticles.

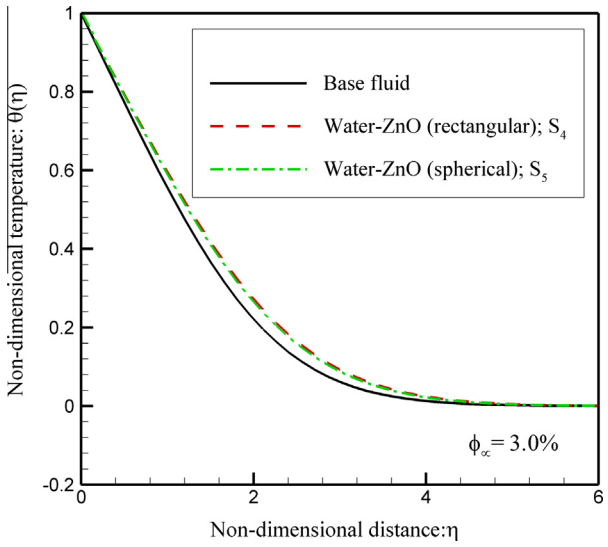

Fig. 8. A comparison between the non-dimensional temperature profiles of ZnO–water nanofluids.

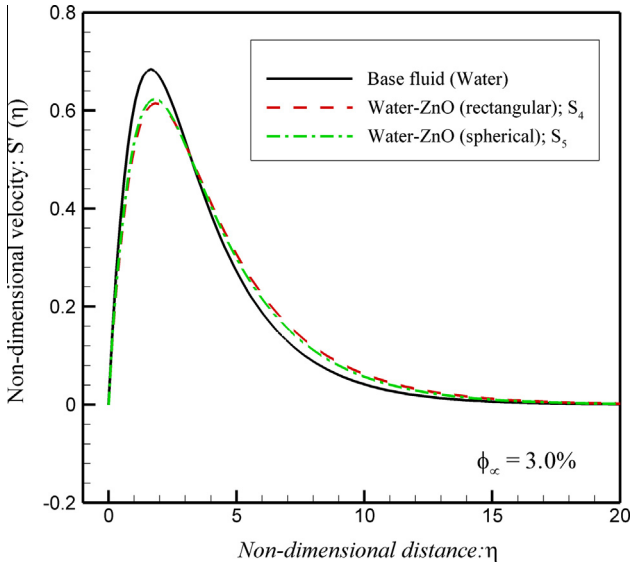

Fig. 7. A comparison between the non-dimensional velocity profiles of water–ZnO nanofluids.

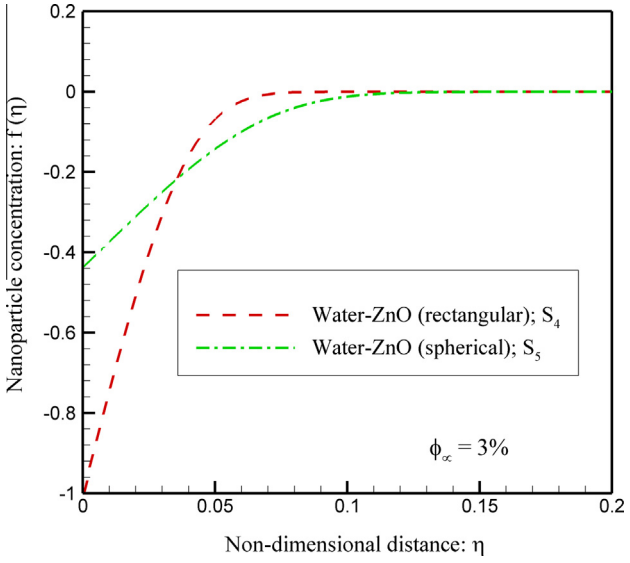

Fig. 9. A comparison between the concentration profiles of water–ZnO nanofluids.

nanoparticles is smoothly higher than that of the rectangular ones. The reason for these behaviors is the fact that the dynamic viscosity parameter of S4 is higher than that of S5. Fig 9 depicts the non-dimensional distribution of nanoparticles in the boundary layer. As seen, the thickness of the concentration boundary layer is very small. This is because of the very high values of Lewis numbers for nanofluids (order of thousands). Table 4 shows that the thermophoresis parameters for both nanofluids (S4 and S5) are the same, but the Brownian motion parameter of S4 is much lower than that of S5. Therefore, the volume fractions of nanoparticles at the surface for S4 is much lower than that of S5. Indeed, for S4, the Brownian motion parameter is very weak, and hence, the thermophoresis force has a tendency to swipe all of the nanoparticles from the vicinity of the surface into the boundary layer. It is also clear that the difference between the thicknesses of the concentration boundary layers is due to the difference between the Lewis numbers of these two studied nanofluids.

Fig. 10 depicts the enhancement ratio of water–ZnO nanofluids as a function of the volume fraction of nanoparticles. This figure shows that the enhancement heat transfer as a result of the presence of rectangular nanoparticles in the base fluid (S4) is higher than that of the spherical ones (S5). Increasing the volume fraction of the spherical nanoparticles smoothly increases the heat transfer enhancement. Table 1 indicates that the thermal conductivity parameter (*Nc*) for the nanofluid containing rectangular nanoparticles is also smoothly higher than the spherical ones.

4.3. Type of nanoparticles

The effect of the types of nanoparticles on the boundary layer and heat transfer of nanofluids is analyzed by comparing the three spherical types of nanoparticles with the approximate diameter of 40 nm. The constrictive materials of nanoparticles are ZnO (S5), MgO (S6) and Al_2O_3 (S7), and the base fluid is water. Figs. 11 and 12 show the non-dimensional velocity and temperature boundary

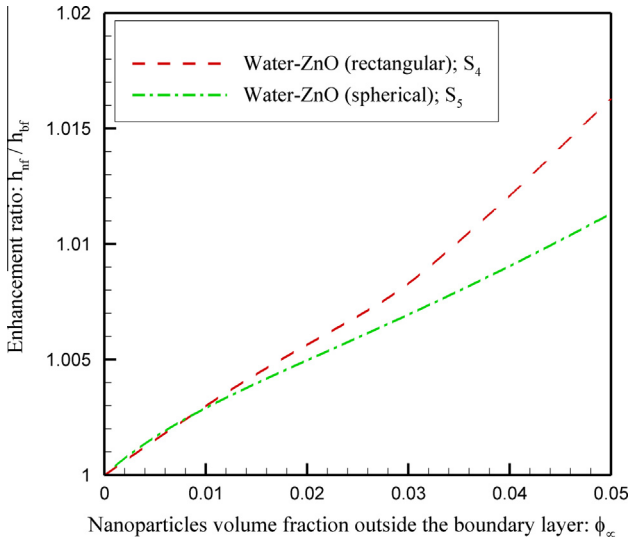

Fig. 10. Enhancement ratio of water–ZnO nanofluids (S4 and S5) as a function of the volume fraction of nanoparticles.

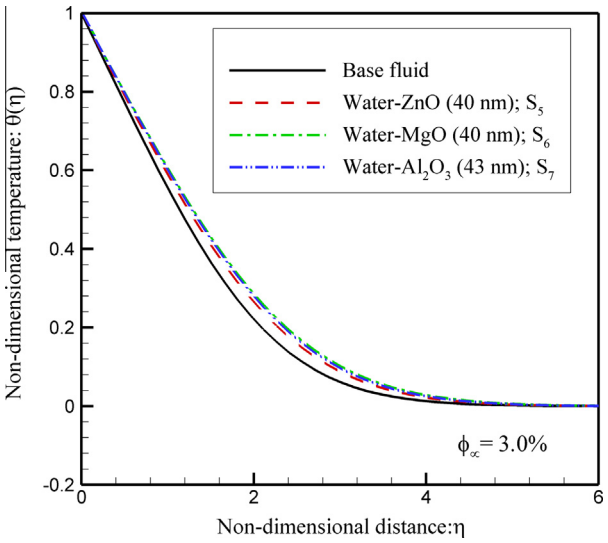

Fig. 12. A comparison between the non-dimensional temperature profiles of different types of nanoparticles.

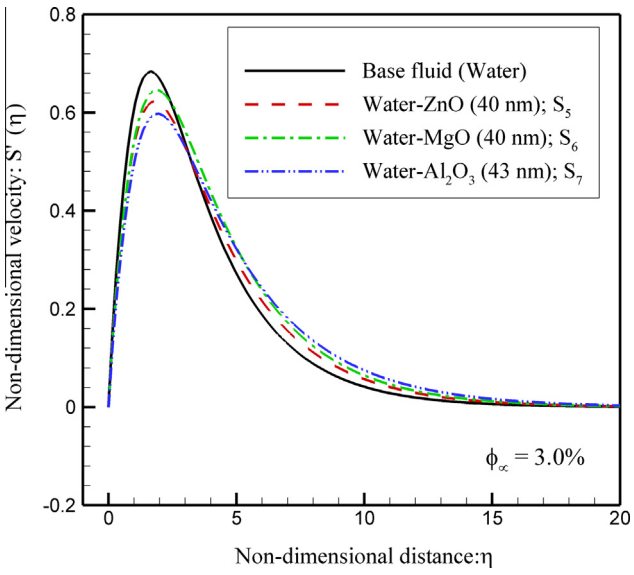

Fig. 11. A comparison between the non-dimensional velocity profiles of different types of nanoparticles.

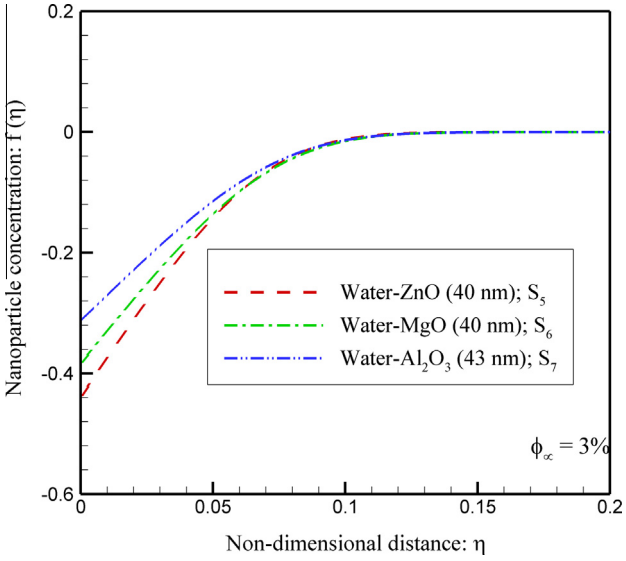

Fig. 13. A comparison between the concentration profiles of different types of nanoparticles.

layer profiles of these nanofluids, respectively. The non-dimensional velocity and temperature profiles of water (the base fluid) are also plotted as a comparison. Fig. 11 shows that the influence of the types of nanoparticles on the hydrodynamic boundary layer is significant. The alumina nanoparticles correspond to the lowest magnitude of the non-dimensional maximum velocity and the highest thickness of the hydrodynamic boundary layer. Fig. 12 indicates that the thickness of the thermal boundary layer of water–ZnO nanofluid is lower than those for the other nanofluids.

Fig. 13 shows the boundary layer concentration profiles of the three types of nanoparticles S5, S6 and S7 over the plate. This figure shows that the difference between the boundary layer concentrations of the different types of nanoparticles is significant. However, the thicknesses of these three boundary layers are almost equal. Table 4 also shows that the Lewis numbers for these nanofluids are almost equal. The lower volume fraction of the nanoparticles at the surface corresponds to the alumina nanoparticles. The difference between the volume fractions of the nanoparticles at the surface is mostly due to the difference between the thermophoresis parameters of these nanofluids.

Fig. 14 shows the enhancement ratio as a function of the volume fraction of nanoparticles for the three different considered types of nanoparticles. As seen, there are three different behaviors. The presence of MgO nanoparticles significantly increases the heat transfer. In contrast, the presence of Al_2O_3 nanoparticles deteriorates the heat transfer. The presence of ZnO nanoparticles almost does not change the heat transfer rate from the plate.

4.4. Type of base fluid

The influence of the type of the base fluid on the boundary layer can be analyzed by comparing the results of S7 and S9. Case S7 is a nanofluid synthesized using 43 nm spherical Al_2O_3 nanoparticles dispersed in water. Case S9 is a nanofluid synthesized using 44 nm spherical Al_2O_3 nanoparticles in kerosene. The non-

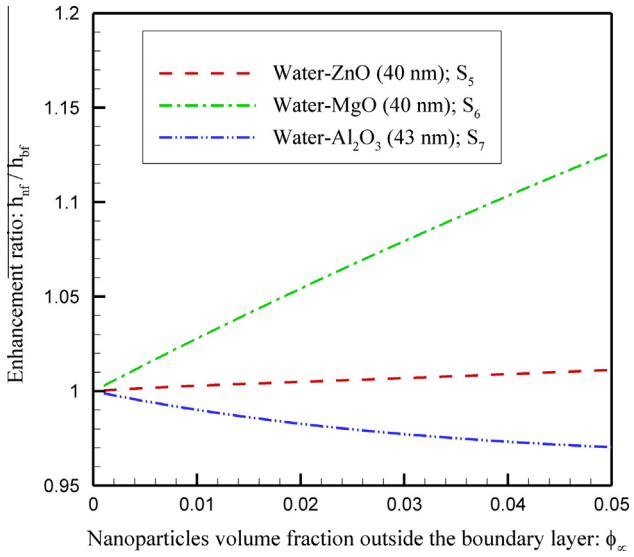

Fig. 14. Enhancement ratio of three types of nanoparticles (S5–S7) as a function of the volume fraction of nanoparticles.

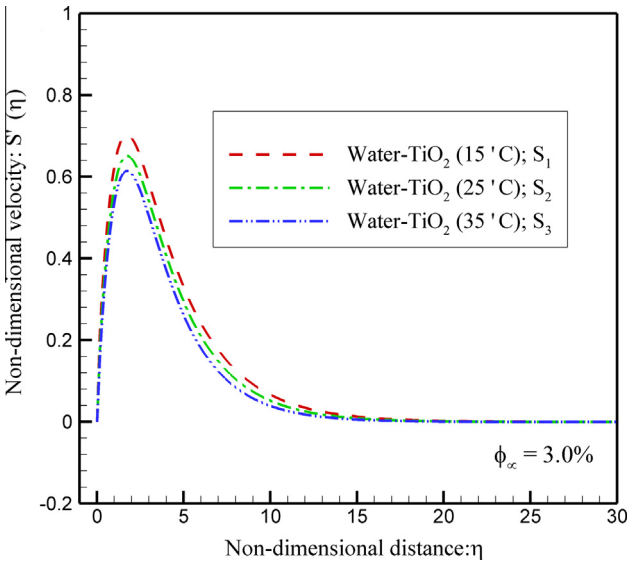

Fig. 15. A comparison between the non-dimensional velocity profiles for different working temperatures.

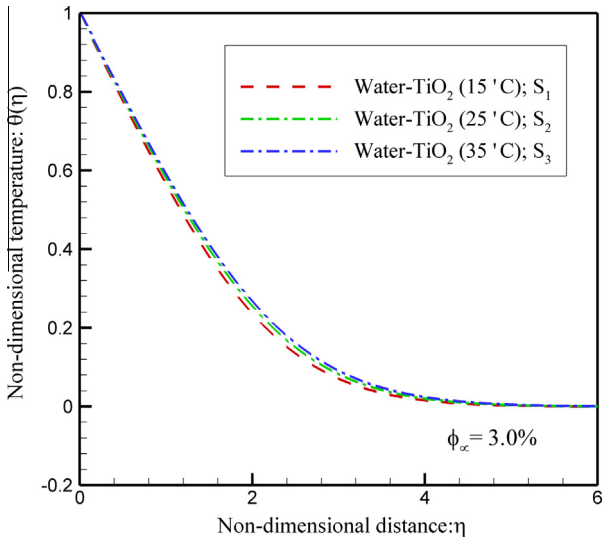

Fig. 16. A comparison between the non-dimensional temperature profiles for different working temperatures.

dimensional boundary layer velocity, temperature and concentration profiles of S7 can be seen in Figs. 11–13, respectively. The enhancement ratio of S7 as a function of the volume fraction of nanoparticles is plotted in Fig. 14. The boundary layer profiles of S9 were plotted in Figs. 3–5. The enhancement ratio of S9 can be seen in Fig. 6. For brevity, the results have not been plotted in new figures here as they are available in the previous figures. A comparison between Figs. 6 and 14 reveals that the base fluid significantly affects the enhancement ratio of the nanofluids. Dispersing the 43 nm alumina nanoparticles in the base fluid of water deteriorates the heat transfer. In contrast, dispersing almost the same nanoparticles in kerosene as the base fluid significantly increases the heat transfer. Therefore, it can be concluded that the type of nanoparticles and the base fluid are two very important factors affecting the heat transfer. Selecting the wrong type of nanoparticles for a base fluid may ultimately result in deterioration of the heat transfer rate. The deterioration and enhancement trends of heat transfer were also previously reported in the experimental studies conducted by Ho et al. [31] and Hu et al. [32]. It was assumed that the reduction of heat transfer could be because of the increase of viscosity or mass transfer mechanisms. The outcomes of the present study indicate that both of the reduction or enhancement of heat transfer can be seen in the trends of the results. These observed reduction or enhancement of heat transfer are under the influence of the viscosity augmentation (*Nv*) as well as the mass transfer mechanism (including *Nr*, *Nb*, *Nt* and *Le*).

4.5. Working temperature

The influence of different working temperatures on the boundary layer profiles and heat transfer is analyzed by comparing three different working temperatures of 15 °C, 25 °C and 35 °C for water–TiO_2 nanofluids containing 21 nm spherical nanoparticles (S1–S3).

Figs. 15 and 16 show the non-dimensional velocity and temperature profiles of water–TiO_2 nanoparticles at different temperatures. Fig. 15 depicts that an increase in the working temperature of the nanofluid decreases the maximum magnitude of the non-dimensional velocity of the nanofluid. Also, increasing the working temperature has the tendency to decrease the thickness of the hydrodynamic boundary layer of the nanofluids. Fig. 16 indicates that the thickness of the thermal boundary layer is an increasing function of the working temperature of the nanofluid. Fig. 17 shows the non-dimensional distribution of nanoparticle in the boundary layer. It is clearly seen that as the working temperature of the nanofluid decreases, the volume fraction of nanoparticles at the surface of the plate also decreases. Therefore, the lower working temperature is the higher migration of the nanoparticles. Fig. 17 also illustrates that increasing the working temperature of nanofluids increases the thickness of the concentration boundary layer. These results are in good agreement with the evaluated non-dimensional parameters in Table 4.

The enhancement ratio as a function of the volume fraction of nanoparticles for different working temperatures of water–TiO_2 nanofluids is plotted in Fig. 18. This figure reveals that increasing the working temperature results in decreasing the enhancement ratio of nanofluids. Therefore, in some critical applications of natural convection of nanofluids, in which the temperature of the system rises, the efficiency of nanofluids decreases. This is a crucial issue in the applications of nanofluids, which has not been pointed out in any of the previous studies of the boundary layer natural convection of nanofluids.

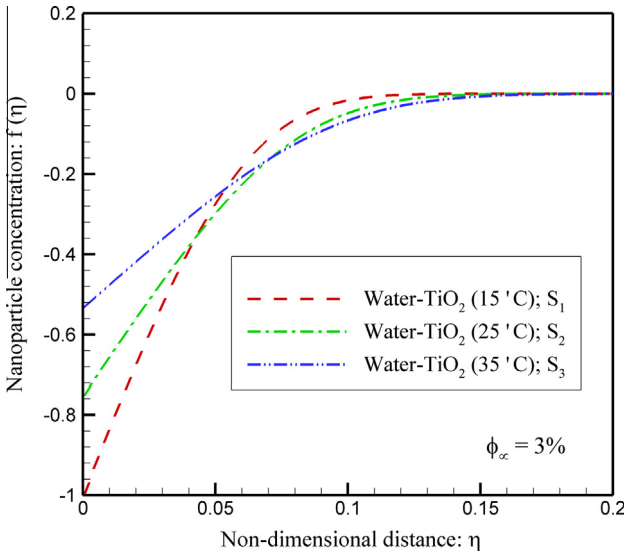

Fig. 17. A comparison between the concentration profiles of profiles for different working temperatures.

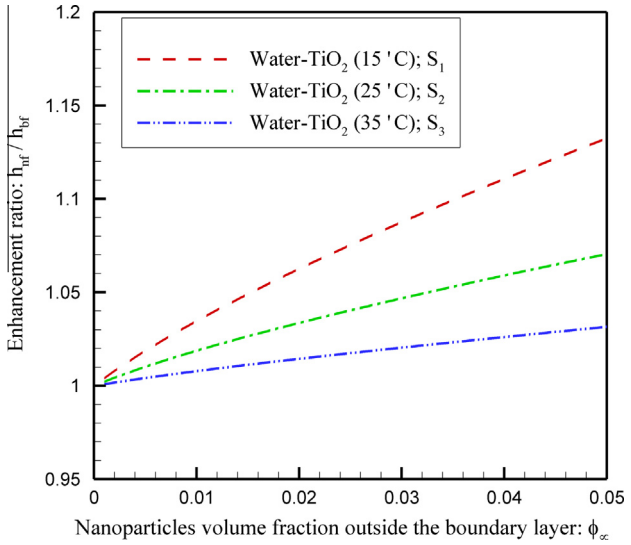

Fig. 18. Enhancement ratio as a function of the volume fraction of nanoparticles for different working temperatures.

5. Conclusion

The natural convection heat and mass transfer of nanofluids over a flat plate was analyzed considering different types of nanoparticles, base fluid and working temperature. The thermal conductivity and the dynamic viscosity of the nanofluids were evaluated using available experimental data. A powerful mathematical approach, the similarity solution approach, was successfully applied. The similarity solution of the problem was obtained considering variable thermal conductivity and dynamic viscosity of nanofluids. The enhanced boundary condition of zero mass flux of nanoparticles at the surface was also successfully utilized. Nine samples of nanofluids from five different studies were selected as case studies. The results of the present study can be summarized as follows:

1. The non-dimensional maximum velocities for nanofluids were lower than those for the base fluids. The presence of nanoparticles in a base fluid increased the thickness of the hydrodynamic boundary layer. The thickness of the thermal boundary layer of a nanofluid was higher than that of the base fluid.
2. The thickness of the concentration boundary layer of nanoparticles was significantly lower than the thicknesses of the thermal or the hydrodynamic boundary layers.
3. The decrease of the size of the nanoparticles significantly increased the heat transfer enhancement. Therefore, the nanoparticles with the smaller sizes were much better than those with larger sizes.
4. The material types of nanoparticles was crucial. The results showed that some nanoparticles can result in significant enhancement of the heat transfer rate, but some nanoparticles can significantly deteriorate the heat transfer from the surface. For example, the dispersion of 40 nm spherical zinc-oxide nanoparticles in water enhance the heat transfer while dispersion of 43 nm spherical alumina nanoparticles in water deteriorated the heat transfer.
5. The type of the base fluid is very important. For example, dispersing 40 nm spherical alumina nanoparticles in kerosene enhanced the natural convection heat transfer while dispersing the same nanoparticles in water deteriorated the natural convection heat transfer. The analysis of the influence of the type of nanoparticles on natural convection boundary layer of nanofluids indicated that the type of nanoparticles also could deteriorate or enhance the natural convection heat transfer. Hence, the type of nanoparticles as well as the type of the base fluid are two important issues, which should be considered simultaneously.
6. The increase of the working temperature of a nanofluid reduces the heat transfer enhancement. Indeed, the dynamic viscosity increased and the thermal conductivity decreased by increasing the working temperature of the nanofluid. The decrease in the efficiency of nanofluids as the result of increasing the working temperature is a very important issue in applications of nanofluids. It means that when a system gets hot and goes into a critical situation, the efficiency of the heat removal of the nanofluids reduces. Hence, this effect needs a sufficient caution in design procedures, and it can limit the potential of nanofluids in reducing the size of industrial heat transfer devices.

Recently, many research publications considered heat transfer of nanofluids in the boundary layer, but only few, practically analyzed the different aspects of the heat transfer of nanofluids with respect to the affective parameters. Some of these affective parameters were addressed in the present study. However, more comprehensive studies for different geometries and different types of nanofluids, are highly demanded. Some other aspects of nanofluids such as the time of sonication, aggregation of nanoparticles, synthesis method and the additives (e.g. surfactants) can also influence the heat transfer enhancement of nanofluids, which are needed to be considered in future studies. In the present study, the effect of different sizes of nanoparticles (non-uniform nanoparticles size) and the effect of the agglomeration of nanoparticles on the thermo-physical properties and the Brownian motion was neglected because of the lack of experimental results and physical models. In the future studies, these effects could be subject of future studies.

Acknowledgements

The second and fourth authors are grateful to Dezful Branch, Islamic Azad University, Dezful, Iran for its financial support. The first, second and fourth authors are acknowledge the Iran Nanotechnology Initiative Council (INIC) for financial support.

The authors would like to thank the very competent Reviewers for the valuable comments and suggestions.

References

[1] S.K. Das, S. Choi, W. Yu, T. Pradeep, Nanofluids: Science and Technology, Wiley Interscience, New Jersey, 2007.

[2] K. Khanafer, K. Vafai, A critical synthesis of thermophysical characteristics of nanofluids, Int. J. Heat Mass Transf. 54 (2011) 4410–4428.

[3] S. Kakaç, A. Pramuanjaroenkij, Review of convective heat transfer enhancement with nanofluids, Int. J. Heat Mass Transf. 52 (2009) 3187–3196.

[4] C. Kleinstreuer, Y. Feng, Experimental and theoretical studies of nanofluid thermal conductivity enhancement: a review, Nanoscale Res. Lett. 6 (2011) 229.

[5] S. Özerinç, S. Kakaç, A. Yazıcıoğlu, Enhanced thermal conductivity of nanofluids: a state-of-the-art review, Microfluid. Nanofluid. 8 (2010) 145–170.

[6] L.S. Sundar, K.V. Sharma, M.T. Naik, M.K. Singh, Empirical and theoretical correlations on viscosity of nanofluids: a review, Renew. Sustain. Energy Rev. 25 (2013) 670–686.

[7] X.-Q. Wang, A.S. Mujumdar, Heat transfer characteristics of nanofluids: a review, Int. J. Therm. Sci. 46 (2007) 1–19.

[8] A. Ghadimi, R. Saidur, H.S.C. Metselaar, A review of nanofluid stability properties and characterization in stationary conditions, Int. J. Heat Mass Transf. 54 (2011) 4051–4068.

[9] A.V. Kuznetsov, D.A. Nield, Natural convective boundary-layer flow of a nanofluid past a vertical plate, Int. J. Therm. Sci. 49 (2010) 243–247.

[10] E. Abu-Nada, A.J. Chamkha, Mixed convection flow in a lid-driven inclined square enclosure filled with a nanofluid, Eur. J. Mech.-B/Fluids 29 (2010) 472–482.

[11] M. Chandrasekar, S. Suresh, A. Chandra Bose, Experimental investigations and theoretical determination of thermal conductivity and viscosity of Al_2O_3/water nanofluid, Exp. Thermal Fluid Sci. 34 (2010) 210–216.

[12] W. Duangthongsuk, S. Wongwises, Measurement of temperature-dependent thermal conductivity and viscosity of TiO_2–water nanofluids, Exp. Thermal Fluid Sci. 33 (2009) 706–714.

[13] J. Jeong, C. Li, Y. Kwon, J. Lee, S.H. Kim, R. Yun, Particle shape effect on the viscosity and thermal conductivity of ZnO nanofluids, Int. J. Refrig 36 (2013) 2233–2241.

[14] H.M. Esfe, S. Saedodin, M. Mahmoodi, Experimental studies on the convective heat transfer performance and thermophysical properties of MgO–water nanofluid under turbulent flow, Exp. Thermal Fluid Sci. 52 (2014) 68–78.

[15] D.K. Agarwal, A. Vaidyanathan, S. Sunil Kumar, Synthesis and characterization of kerosene–alumina nanofluids, Appl. Therm. Eng. 60 (2013) 275–284.

[16] J. Buongiorno, D.C. Venerus, N. Prabhat, T. McKrell, J. Townsend, R. Christianson, et al., A benchmark study on the thermal conductivity of nanofluids, J. Appl. Phys. 106 (2009) 094312.

[17] D.C. Venerus, J. Buongiorno, R. Christianson, J. Townsend, I.C. Bang, G. Chen, et al., Viscosity measurements on colloidal dispersions (nanofluids) for heat transfer applications, Appl. Rheol. 20 (2010) 44582.

[18] P. Rana, R. Bhargava, Numerical study of heat transfer enhancement in mixed convection flow along a vertical plate with heat source/sink utilizing nanofluids, Commun. Nonlinear Sci. Numer. Simul. 16 (2011) 4318–4334.

[19] A. Aziz, W.A. Khan, Natural convective boundary layer flow of a nanofluid past a convectively heated vertical plate, Int. J. Therm. Sci. 52 (2012) 83–90.

[20] M.J. Uddin, W.A. Khan, A.I. Ismail, MHD free convective boundary layer flow of a nanofluid past a flat vertical plate with Newtonian heating boundary condition, PLoS ONE 7 (2012) e49499.

[21] A.V. Kuznetsov, D.A. Nield, Natural convective boundary-layer flow of a nanofluid past a vertical plate: a revised model, Int. J. Therm. Sci. 77 (2014) 126–129.

[22] M. Chandrasekar, S. Suresh, A review on the mechanisms of heat transport in nanofluids, Heat Transfer Eng. 30 (2009) 1136–1150.

[23] J. Sarkar, A critical review on convective heat transfer correlations of nanofluids, Renew. Sustain. Energy Rev. 15 (2011) 3271–3277.

[24] W. Yu, D.M. France, J.L. Routbort, S.U. Choi, Review and comparison of nanofluid thermal conductivity and heat transfer enhancements, Heat Transfer Eng. 29 (2008) 432–460.

[25] J. Buongiorno, Convective transport in nanofluids, J. Heat Transfer 128 (2006) 240.

[26] U.M. Ascher, R. Mattheij, R. Russell, Numerical Solution of Boundary Value Problems for Ordinary Differential Equations, second ed., SIAM, Philadelphia, USA, 1995.

[27] R.D. Russell, L.F. Shampine, A collocation method for boundary value problems, Numer. Math. 19 (1972) 1–28.

[28] E. ToolBox, Constant Pressure Heat Capacity of Water vs. Temperature. <http://www.engineeringtoolbox.com/water-thermal-properties-d_162.html>, 2013 (retrieved 01.11.13).

[29] E. ToolBox, Fuels, Densities and Specific Volumes Properties. <www.engineeringtoolbox.com/fuels-densities-specific-volumes-d_166.html>, 2013 (retrieved 01.11.13).

[30] S.D.B. Ceramaret, Physical mechanical thermal, electrical and chemical properties (2013).

[31] C.J. Ho, W.K. Liu, Y.S. Chang, C.C. Lin, Natural convection heat transfer of alumina–water nanofluid in vertical square enclosures: an experimental study, Int. J. Therm. Sci. 49 (2010) 1345–1353.

[32] Y. Hu, Y. He, C. Qi, B. Jiang, H.I. Schlaberg, Experimental and numerical study of natural convection in a square enclosure filled with nanofluid, Int. J. Heat Mass Transf. 78 (2014) 380–392.